

Article

Elastic Properties and Energy Loss Related to the Disorder–Order Ferroelectric Transitions in Multiferroic Metal–Organic Frameworks $[\text{NH}_4][\text{Mg}(\text{HCOO})_3]$ and $[(\text{CH}_3)_2\text{NH}_2][\text{Mg}(\text{HCOO})_3]$

Zhiying Zhang *, Hongliang Yu, Xin Shen, Lei Sun, Shumin Yue and Hao Tang

School of Materials Science and Engineering, Wuhan University of Technology, Wuhan 430070, China; yuhongliang2021@126.com (H.Y.); shenxin1221@126.com (X.S.); sunlei15171@163.com (L.S.); yueshumin1216@163.com (S.Y.); tanghao202103@163.com (H.T.)

* Correspondence: zhiyingzhang@whut.edu.cn

Abstract: Elastic properties are important mechanical properties which are dependent on the structure, and the coupling of ferroelasticity with ferroelectricity and ferromagnetism is vital for the development of multiferroic metal–organic frameworks (MOFs). The elastic properties and energy loss related to the disorder–order ferroelectric transition in $[\text{NH}_4][\text{Mg}(\text{HCOO})_3]$ and $[(\text{CH}_3)_2\text{NH}_2][\text{Mg}(\text{HCOO})_3]$ were investigated using differential scanning calorimetry (DSC) and dynamic mechanical analysis (DMA). The DSC curves of $[\text{NH}_4][\text{Mg}(\text{HCOO})_3]$ and $[(\text{CH}_3)_2\text{NH}_2][\text{Mg}(\text{HCOO})_3]$ exhibited anomalies near 256 K and 264 K, respectively. The DMA results illustrated the minimum in the storage modulus and normalized storage modulus, and the maximum in the loss modulus, normalized loss modulus and loss factor near the ferroelectric transition temperatures of 256 K and 264 K, respectively. Much narrower peaks of loss modulus, normalized loss modulus and loss factor were observed in $[(\text{CH}_3)_2\text{NH}_2][\text{Mg}(\text{HCOO})_3]$ with the peak temperature independent of frequency, and the peak height was smaller at a higher frequency, indicating the features of first-order transition. Elastic anomalies and energy loss in $[\text{NH}_4][\text{Mg}(\text{HCOO})_3]$ near 256 K are due to the second-order paraelectric to ferroelectric phase transition triggered by the disorder–order transition of the ammonium cations and their displacement within the framework channels, accompanied by the structural phase transition from the non-polar hexagonal $P6_322$ to polar hexagonal $P6_3$. Elastic anomalies and energy loss in $[(\text{CH}_3)_2\text{NH}_2][\text{Mg}(\text{HCOO})_3]$ near 264 K are due to the first-order paraelectric to ferroelectric phase transitions triggered by the disorder–order transitions of alkylammonium cations located in the framework cavities, accompanied by the structural phase transition from rhombohedral $R\bar{3}c$ to monoclinic Cc . The elastic anomalies in $[\text{NH}_4][\text{Mg}(\text{HCOO})_3]$ and $[(\text{CH}_3)_2\text{NH}_2][\text{Mg}(\text{HCOO})_3]$ showed strong coupling of ferroelasticity with ferroelectricity.

Keywords: metal–organic framework (MOF); ferroelectric transition; dynamic mechanical analysis (DMA); elastic property; energy loss



Citation: Zhang, Z.; Yu, H.; Shen, X.; Sun, L.; Yue, S.; Tang, H. Elastic Properties and Energy Loss Related to the Disorder–Order Ferroelectric Transitions in Multiferroic Metal–Organic Frameworks $[\text{NH}_4][\text{Mg}(\text{HCOO})_3]$ and $[(\text{CH}_3)_2\text{NH}_2][\text{Mg}(\text{HCOO})_3]$. *Materials* **2021**, *14*, 3125. <https://doi.org/10.3390/ma14113125>

Academic Editor: Lucia Carlucci

Received: 5 May 2021

Accepted: 2 June 2021

Published: 7 June 2021

Publisher's Note: MDPI stays neutral with regard to jurisdictional claims in published maps and institutional affiliations.



Copyright: © 2021 by the authors. Licensee MDPI, Basel, Switzerland. This article is an open access article distributed under the terms and conditions of the Creative Commons Attribution (CC BY) license (<https://creativecommons.org/licenses/by/4.0/>).

1. Introduction

Metal–organic frameworks (MOFs) have attracted intensive attention due to their tunable properties and potential applications in gas storage and separations, catalysis, photoluminescence, sensors, magnetic and electric applications [1–7]. Multiferroic MOFs with at least two coexisting orders among the ferroelectricity, ferromagnetism and ferroelasticity are of particular interest, and their structure analysis, thermal properties, electric properties and magnetic properties have been widely studied using X-ray diffraction (XRD), neutron scattering, infrared spectroscopy, Raman spectroscopy, differential scanning calorimetry (DSC), heat capacity measurements, dielectric measurements, magnetic measurements and computer simulations [8–14].

In $[\text{NH}_4][\text{M}(\text{HCOO})_3]$ ($\text{M} = \text{Mg}, \text{Mn}, \text{Fe}, \text{Co}, \text{Ni}, \text{Zn}$), paraelectric to ferroelectric phase transitions triggered by the disorder–order transitions of the ammonium cations and their displacement within the framework channels occur between 191 K and 255 K (Co: 191 K, Zn: 192 K, Ni: 199 K, Fe: 212 K, Mn: 254 K, Mg: 255 K), accompanied by the structural phase transition from the non-polar hexagonal space group $P6_322$ to the polar hexagonal space group $P6_3$ [15–27]. Moreover, in $[\text{NH}_4][\text{M}(\text{HCOO})_3]$ ($\text{M} = \text{Mn}, \text{Fe}, \text{Co}, \text{Ni}$), spin-canted antiferromagnetic ordering ($\text{M} = \text{Mn}, \text{Co}, \text{Ni}$) or ferromagnetic ordering ($\text{M} = \text{Fe}$) occurs between 8 K and 30 K (Mn: 8.4 K, Fe: 9.4 K, Co: 9.8 K, Ni: 29.5 K), indicating the existence of magnetoelectric coupling [20–27]. According to first-principle calculations, it is predicted that magnetism and ferroelectricity also coexist in $[\text{NH}_4][\text{M}(\text{HCOO})_3]$ ($\text{M} = \text{Sc}, \text{Ti}, \text{V}, \text{Cr}, \text{Cu}$) [28].

In $[(\text{CH}_3)_2\text{NH}_2][\text{M}(\text{HCOO})_3]$ ($\text{M} = \text{Mg}, \text{Mn}, \text{Fe}, \text{Co}, \text{Ni}, \text{Zn}$), the paraelectric–ferroelectric phase transitions triggered by the order–disorder of the alkylammonium cations located in the framework cavities occur at 156 K–267 K (Zn: 156 K, Fe: 160 K, Co: 165 K, Ni: 180 K, Mn: 185 K, Mg: 267 K), associated with a structural phase transition from rhombohedral $R\bar{3}c$ to monoclinic Cc [29–41]. The ferroelectric transition temperature is the highest when M is Mg , because Mg^{2+} is the hardest Lewis acid among them, leading to the strongest hydrogen bonds [35]. Furthermore, the spin-canted antiferromagnetic ordering transitions in $[(\text{CH}_3)_2\text{NH}_2][\text{M}(\text{HCOO})_3]$ ($\text{M} = \text{Mn}, \text{Co}, \text{Ni}, \text{Fe}, \text{Cu}$) occur below 40 K (Ni: 35.6 K, Fe: 20 K, Co: 14.9 K, Mn: 8.5 K, Cu: 5.2 K) due to the metal ions within the framework skeletons, and the spin reorientation transitions in $[(\text{CH}_3)_2\text{NH}_2][\text{M}(\text{HCOO})_3]$ ($\text{M} = \text{Co}, \text{Ni}$) occur at 13.1–14.3 K (Co: 13.1 K, Ni: 14.3 K) [42–53]. The effect of pressure on the structure and the electric and magnetic properties of $[(\text{CH}_3)_2\text{NH}_2][\text{M}(\text{HCOO})_3]$ ($\text{M} = \text{Mg}, \text{Mn}, \text{Co}, \text{Zn}, \text{Cd}$) was investigated [37,47,54–56].

The ferroelectric transition temperatures of $[\text{NH}_4][\text{Mg}(\text{HCOO})_3]$ and $[(\text{CH}_3)_2\text{NH}_2][\text{Mg}(\text{HCOO})_3]$ are around 255 K and 267 K, respectively, close to room temperature, leading to promising applications. Their synthesis, structure analysis, thermal properties, dielectric properties, IR studies and Raman studies have been well studied [13–15,33–38,57,58]. However, their elastic properties have not been reported. The present work studied the elastic properties and energy loss of $[\text{NH}_4][\text{Mg}(\text{HCOO})_3]$ and $[(\text{CH}_3)_2\text{NH}_2][\text{Mg}(\text{HCOO})_3]$ associated with ferroelectric transitions using dynamic mechanical analysis (DMA) at low frequencies of 0.1–10 Hz and at high stress and strain levels and investigated the relationship between the structure of MOFs and their elastic properties. The findings quantified the changes in elastic properties and energy loss related to the ferroelectric phase transition and contributed to the further understanding of the phase transition mechanism.

2. Materials and Methods

2.1. Material Synthesis

Single crystals of $[\text{NH}_4][\text{Mg}(\text{HCOO})_3]$ and $[(\text{CH}_3)_2\text{NH}_2][\text{Mg}(\text{HCOO})_3]$ were synthesized by the slow diffusion methods described in [15] and [37], respectively. To obtain crystals of $[\text{NH}_4][\text{Mg}(\text{HCOO})_3]$, a 16 mL methanol solution containing 12.8 mmol $[\text{NH}_4][\text{HCOO}]$ and 12.8 mmol HCOOH was placed at the bottom of a tube, and then a 16 mL methanol solution containing 1.6 mmol of MgCl_2 was gently added. The tube was sealed and kept undisturbed, and colorless crystals of $[\text{NH}_4][\text{Mg}(\text{HCOO})_3]$ were harvested after 1 week. To obtain crystals of $[(\text{CH}_3)_2\text{NH}_2][\text{Mg}(\text{HCOO})_3]$, a 10 mL methanol solution containing 6 mmol of dimethylamine and 8 mmol of formic acid was placed at the bottom of a tube, and then a 16 mL methanol solution containing 2 mmol MgCl_2 was gently added. The tube was sealed and kept undisturbed, and colorless crystals of $[(\text{CH}_3)_2\text{NH}_2][\text{Mg}(\text{HCOO})_3]$ were harvested after 1 week. The crystals were filtered from the mother liquid and washed in ethanol 5 times.

2.2. Morphology

The morphology of the $[\text{NH}_4][\text{Mg}(\text{HCOO})_3]$ and $[(\text{CH}_3)_2\text{NH}_2][\text{Mg}(\text{HCOO})_3]$ crystals were examined by SH11/YF9 (ZhongXi, Beijing, China) optical microscopy (OM) and JSM-IT300 (JOEL, Tokyo, Japan) scanning electron microscopy (SEM).

2.3. Powder XRD

The powder XRD patterns of $[\text{NH}_4][\text{Mg}(\text{HCOO})_3]$ and $[(\text{CH}_3)_2\text{NH}_2][\text{Mg}(\text{HCOO})_3]$ were collected through a Bruker D8 Advance diffractometer (Bruker, Billerica, MA, USA) using $\text{Cu K}\alpha$ radiation with a wavelength of 1.5406 \AA at 40 kV and 40 mA. The diffraction angle 2θ was in the range of $10\text{--}60^\circ$ and the step size was 0.02° . The Rietveld fit of the XRD patterns was obtained using GSAS.

2.4. DSC

The DSC measurements of $[\text{NH}_4][\text{Mg}(\text{HCOO})_3]$ and $[(\text{CH}_3)_2\text{NH}_2][\text{Mg}(\text{HCOO})_3]$ (around 10 mg) were performed through Netzsch DSC 200F3 (Netzsch, Selb, Germany) in the range of 200–300 K during cooling and heating processes at the rate of 5 K/min.

2.5. DMA

DMA measurements of the single crystals of $[\text{NH}_4][\text{Mg}(\text{HCOO})_3]$ and $[(\text{CH}_3)_2\text{NH}_2][\text{Mg}(\text{HCOO})_3]$ were carried out using DMA8000 instruments (PerkinElmer Instruments, Waltham, MA, USA) in the single cantilever mode from 160 K to 320 K at the rate of 2 K/min. DMA measurements of pellets of $[\text{NH}_4][\text{Mg}(\text{HCOO})_3]$ and $[(\text{CH}_3)_2\text{NH}_2][\text{Mg}(\text{HCOO})_3]$ were carried out in the compression mode using PerkinElmer Instruments Diamond DMA (PerkinElmer Instruments, Waltham, MA, USA) in the range of 140–300 K at 2 K/min during heating processes, as described in [39,53].

3. Results and Discussion

3.1. Morphology

The OM and SEM images of $[\text{NH}_4][\text{Mg}(\text{HCOO})_3]$ and $[(\text{CH}_3)_2\text{NH}_2][\text{Mg}(\text{HCOO})_3]$ crystals are illustrated in Figures 1 and 2. The sizes of $[\text{NH}_4][\text{Mg}(\text{HCOO})_3]$ and $[(\text{CH}_3)_2\text{NH}_2][\text{Mg}(\text{HCOO})_3]$ crystals are around 0.2 mm and 0.5 mm, respectively.

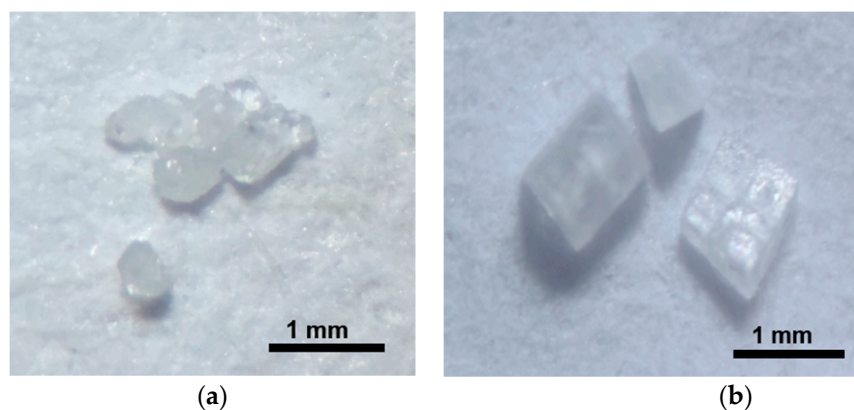


Figure 1. OM image of (a) $[\text{NH}_4][\text{Mg}(\text{HCOO})_3]$ and (b) $[(\text{CH}_3)_2\text{NH}_2][\text{Mg}(\text{HCOO})_3]$ crystals.

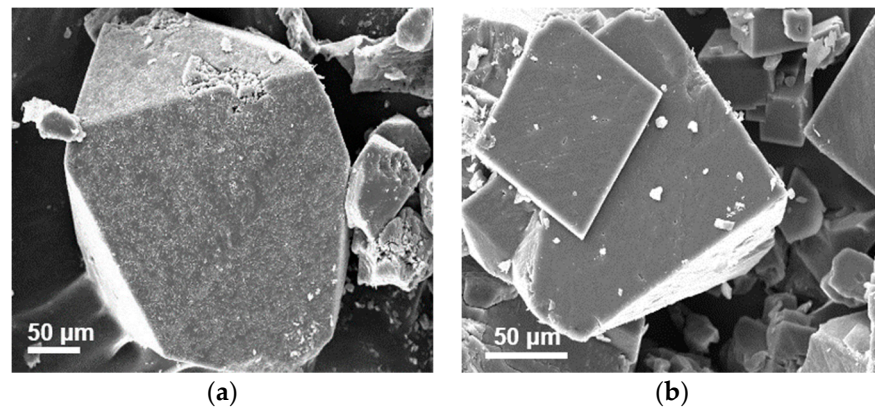


Figure 2. SEM image of (a) $[\text{NH}_4][\text{Mg}(\text{HCOO})_3]$ and (b) $[(\text{CH}_3)_2\text{NH}_2][\text{Mg}(\text{HCOO})_3]$ crystals.

3.2. Powder XRD

The experimental powder XRD pattern of $[\text{NH}_4][\text{Mg}(\text{HCOO})_3]$ at room temperature is consistent with the simulated XRD pattern of the non-polar hexagonal space group $P6_322$ (CCDC 949604), as demonstrated in Figure 3a. The lattice parameters obtained by Rietveld refinement are $a = b = 7.2729(3) \text{ \AA}$, $c = 8.2104(5) \text{ \AA}$, $\alpha = \beta = 90^\circ$, $\gamma = 120^\circ$, $R_{\text{wp}} = 15.53\%$ and $R_{\text{p}} = 11.38\%$. These results agree with the results reported by Maczka et al. [15], which were $a = b = 7.8230(10) \text{ \AA}$, $c = 8.2240(16) \text{ \AA}$, $\alpha = \beta = 90^\circ$ and $\gamma = 120^\circ$.

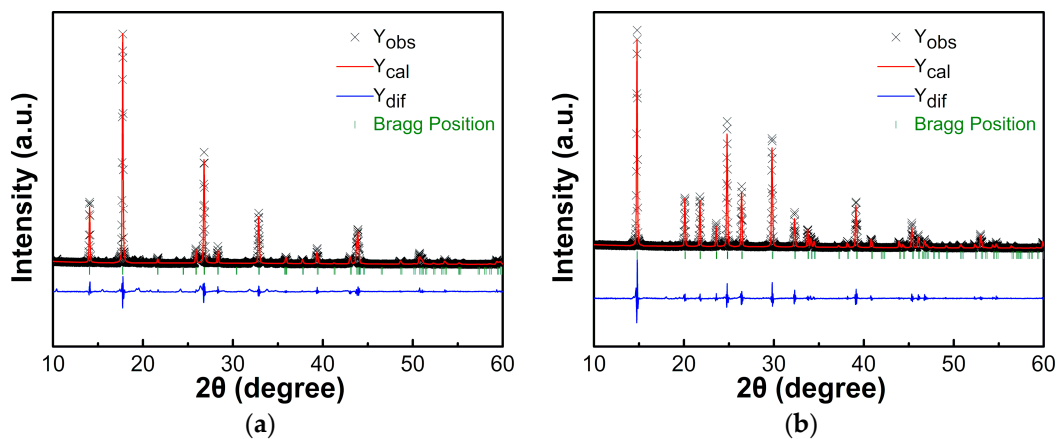


Figure 3. Rietveld fit of XRD patterns of (a) $[\text{NH}_4][\text{Mg}(\text{HCOO})_3]$ and (b) $[(\text{CH}_3)_2\text{NH}_2][\text{Mg}(\text{HCOO})_3]$ at room temperature.

The experimental powder XRD pattern of $[(\text{CH}_3)_2\text{NH}_2][\text{Mg}(\text{HCOO})_3]$ at room temperature is consistent with the simulated XRD pattern of the space group rhombohedral $R\bar{3}c$ (CCDC 696736), as shown in Figure 3b. The refined lattice parameters are $a = b = 8.1525(1) \text{ \AA}$, $c = 22.6015(6) \text{ \AA}$, $\alpha = \beta = 90^\circ$, $\gamma = 120^\circ$, $R_{\text{wp}} = 11.69\%$ and $R_{\text{p}} = 9.09\%$. These are consistent with the results reported by Rossin et al. [33] which were $a = b = 8.149(3) \text{ \AA}$, $c = 22.598(3) \text{ \AA}$, $R_{\text{wp}} = 4.71\%$ and $R_{\text{p}} = 12.03\%$.

The structures of $[\text{NH}_4][\text{Mg}(\text{HCOO})_3]$ and $[(\text{CH}_3)_2\text{NH}_2][\text{Mg}(\text{HCOO})_3]$ at room temperature are demonstrated in Figure 4.

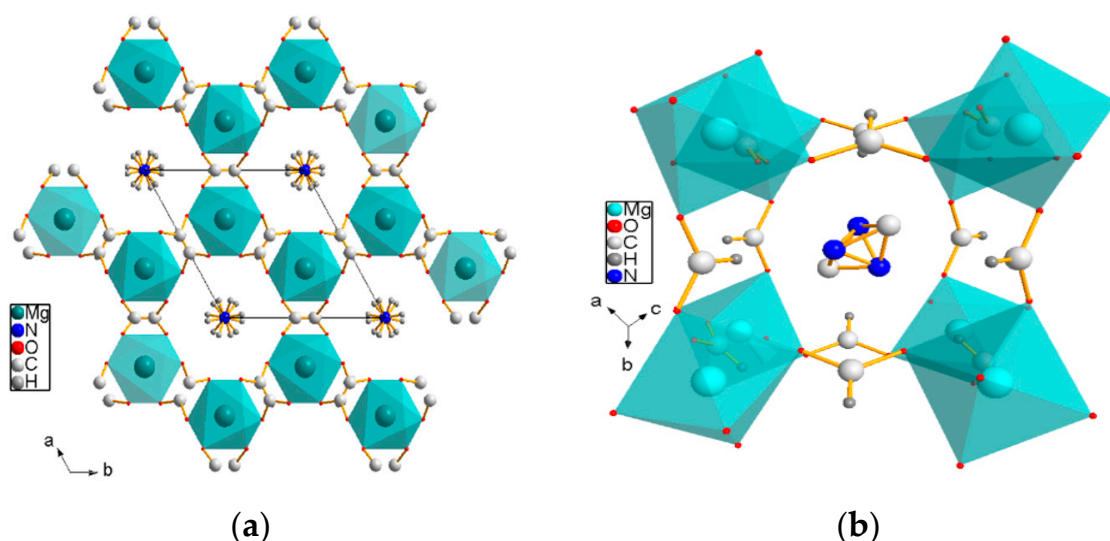


Figure 4. Structures of (a) $[\text{NH}_4][\text{Mg}(\text{HCOO})_3]$ and (b) $[(\text{CH}_3)_2\text{NH}_2][\text{Mg}(\text{HCOO})_3]$ at room temperature.

3.3. DSC

Figure 5a displays the DSC curves of $[\text{NH}_4][\text{Mg}(\text{HCOO})_3]$ with anomalies at 254–256 K at the cooling and heating rate of 5 K/min. This agrees with the transition temperature of 254–255 K reported by Maczka et al. at the rate of 15 K/min [15]. The enthalpy ΔH was determined to be $53.0 - 62.4 \text{ J}\cdot\text{mol}^{-1}$ and the entropy ΔS was determined to be $0.246 - 0.207 \text{ J}\cdot\text{mol}^{-1}\cdot\text{K}^{-1}$. The ratio of the number of configurations in the disordered and ordered systems, N , was determined to be 1.025–1.030. It suggests that the transition is more complex than a simple 3-fold order–disorder model, with N around 3. Maczka et al. reported that the λ -type anomaly in the DSC curve indicated that the ferroelectric transition in $[\text{NH}_4][\text{Mg}(\text{HCOO})_3]$ was second order [15]. Variable-temperature Raman spectra indicated no obvious jumps in the characteristic peak positions of the vibration groups near the transition temperature, indicating the nature of the second-order phase transition [19,22].

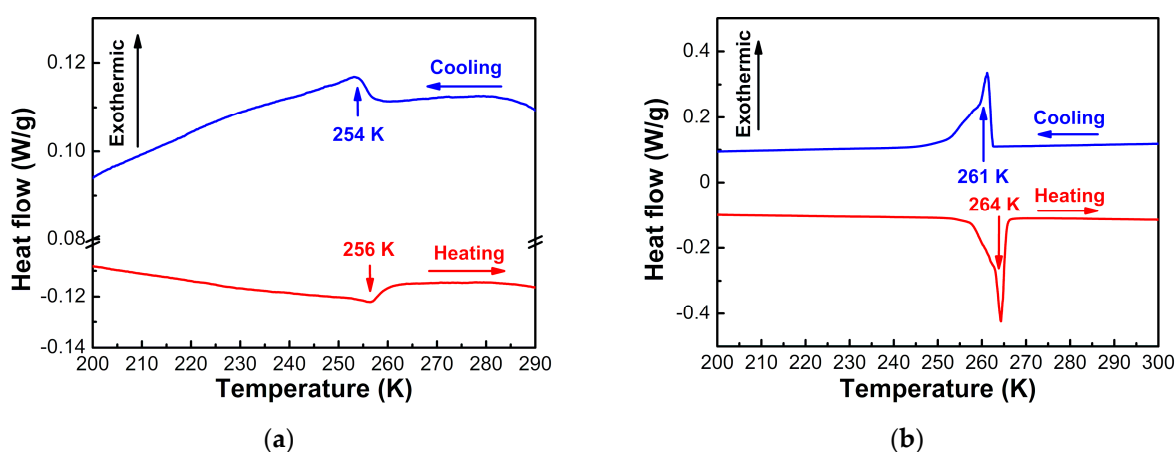


Figure 5. DSC curves of (a) $[\text{NH}_4][\text{Mg}(\text{HCOO})_3]$ and (b) $[(\text{CH}_3)_2\text{NH}_2][\text{Mg}(\text{HCOO})_3]$ during cooling and heating processes at the rate of 5 K/min.

Figure 5b illustrates the DSC curves of $[(\text{CH}_3)_2\text{NH}_2][\text{Mg}(\text{HCOO})_3]$ with anomalies at 261–264 K at the cooling and heating rate of 5 K/min. This is consistent with the transition temperatures of 258–263 K reported by Pato-Doldan et al. [35] and 259–267 K reported by Asaji et al. [36]. The enthalpy ΔH was determined to be $2.596 - 2.723 \text{ kJ}\cdot\text{mol}^{-1}$, and the

entropy ΔS was determined to be $9.8\text{--}10.4\text{ J}\cdot\text{mol}^{-1}\cdot\text{K}^{-1}$. N was determined to be $3.25\text{--}3.49$, indicating a 3-fold order–disorder model for the dimethylammonium cation. Asaji et al. reported similar values of ΔH , $2.7 \pm 0.2\text{ kJ}\cdot\text{mol}^{-1}$ and ΔS , $10 \pm 1\text{ J}\cdot\text{mol}^{-1}\cdot\text{K}^{-1}$ [36].

3.4. DMA

DMA was used to determine the complex modulus of the viscoelastic materials. The real part is the storage modulus E' , the imaginary part is the loss modulus E'' , and E''/E' is the loss factor $\tan\delta$. The temperature dependence of the storage modulus E' , loss modulus E'' and loss factor $\tan\delta$ of $[\text{NH}_4][\text{Mg}(\text{HCOO})_3]$ single crystals are exhibited in Figure 6a–c, and the temperature dependences of the normalized storage modulus E'_T/E'_{280} (i.e., the ratio of the storage modulus at temperature T to that at 280 K), normalized loss modulus E''_T/E''_{298} (i.e., the ratio of the loss modulus at temperature T to that at 280 K) and loss factor $\tan\delta$ of the $[\text{NH}_4][\text{Mg}(\text{HCOO})_3]$ pellet are illustrated in Figure 6d–f. With the increase in temperature, the storage modulus of the single crystals and the normalized storage modulus of the pellet gradually decreased, reaching the minimum near the ferroelectric transition temperature of 256 K, and then gradually increased. With the increase in temperature, the loss modulus and loss factor of the $[\text{NH}_4][\text{Mg}(\text{HCOO})_3]$ single crystals and the normalized loss modulus and loss factor of the $[\text{NH}_4][\text{Mg}(\text{HCOO})_3]$ pellet gradually increased, reaching the maximum near 256 K, and then slightly decreased. The peaks of loss modulus, normalized loss modulus and loss factor are broad, and they indicate weak frequency dependence.

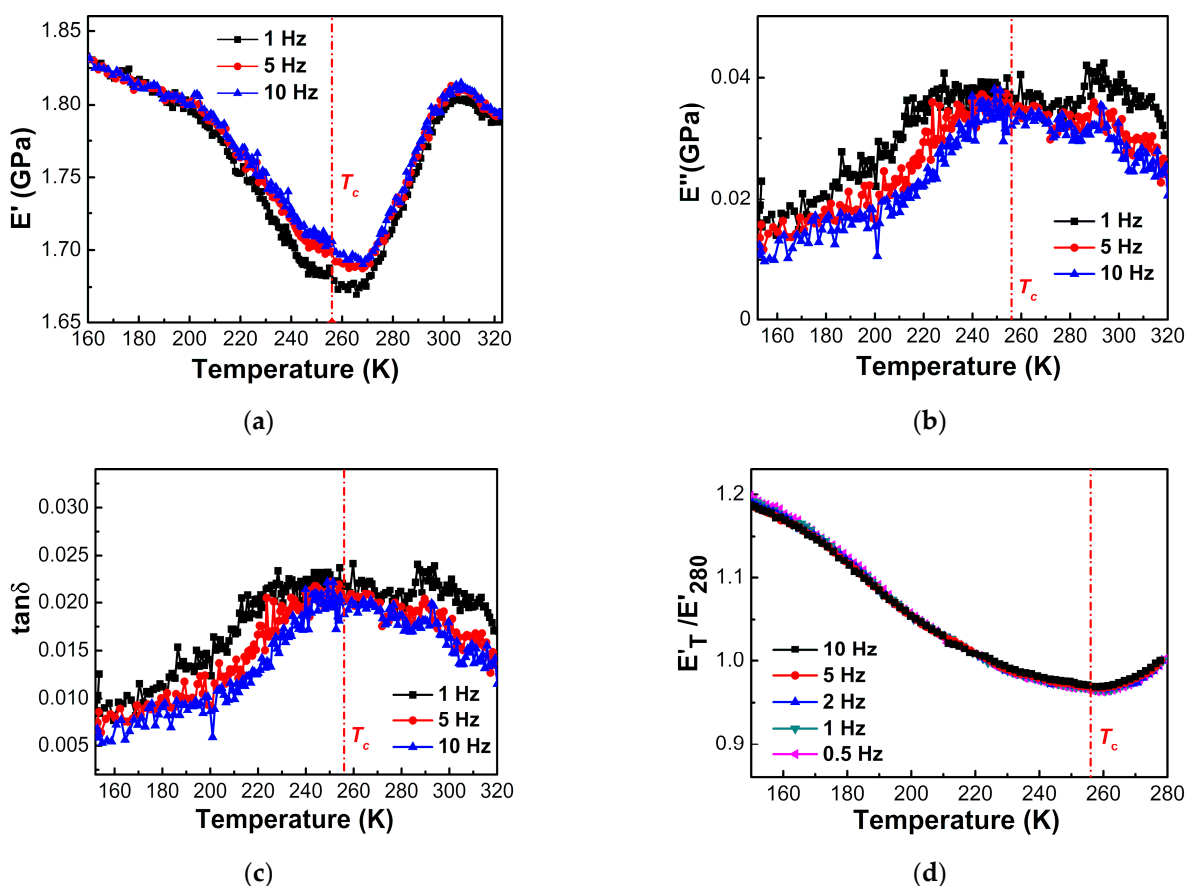


Figure 6. Cont.

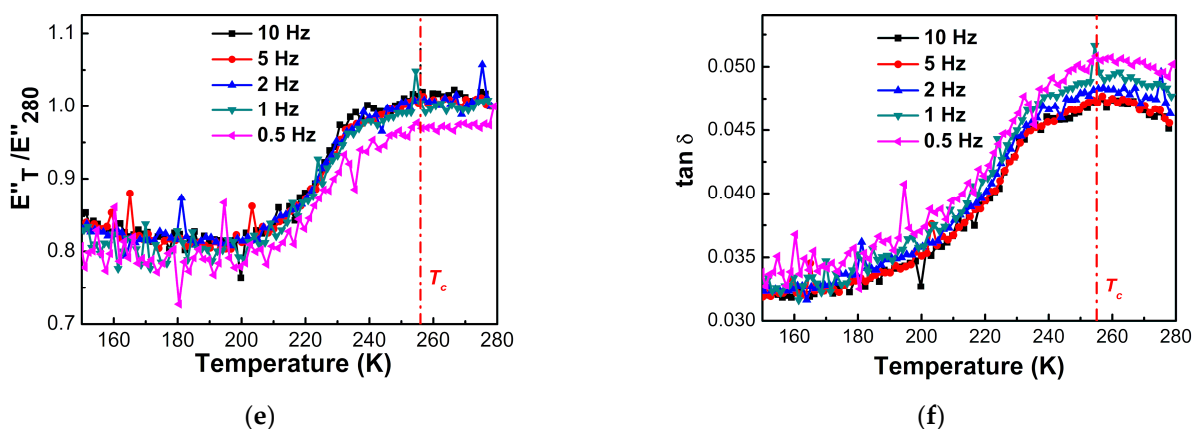


Figure 6. Temperature dependences of (a) storage modulus E' , (b) loss modulus E'' , (c) loss factor $\tan\delta$ of $[\text{NH}_4][\text{Mg}(\text{HCOO})_3]$ single crystals, (d) normalized storage modulus E'_T/E'_{280} , (e) normalized loss modulus E''_T/E''_{280} and (f) loss factor $\tan\delta$ of $[\text{NH}_4][\text{Mg}(\text{HCOO})_3]$ pellet determined by DMA during heating at the rate of 2 K/min. The vertical dash-dotted line indicates the ferroelectric transition temperature of 256 K.

A broad dielectric anomaly was reported in the temperature dependences of the dielectric constant for $[\text{NH}_4][\text{Mg}(\text{HCOO})_3]$, and the peak position demonstrated slight frequency dependence [15]. The resonant ultrasound spectroscopy (RUS) study of the elastic properties and acoustic dissipation associated with the disorder–order ferroelectric transition in $[\text{NH}_4][\text{Zn}(\text{HCOO})_3]$ exhibited that, with the increase in temperature, the elastic moduli, which were proportional to the square of the resonant frequencies, gradually decreased. There was also a marked change in the rate of decrease near the ferroelectric transition temperature of 192 K, and acoustic dissipation gradually increased with a peak near 192 K [16]. The Brillouin scattering (BS) study of the elastic properties and acoustic dissipation associated with the ferroelectric transition in $[\text{NH}_4][\text{M}(\text{HCOO})_3]$ ($\text{M} = \text{Mn}, \text{Zn}$) displayed that, with the increase in temperature, the frequency shift for the longitudinal and transverse acoustic phonons propagating along the x axis gradually decreased, and anomalies occurred near the ferroelectric transition temperature, with an estimated relaxation time around 4.6×10^{-13} s [22].

Figure 7 illustrates the temperature dependence of storage modulus E' , loss modulus E'' and loss factor $\tan\delta$ of the $[(\text{CH}_3)_2\text{NH}_2][\text{Mg}(\text{HCOO})_3]$ single crystals, and the normalized storage modulus E'_T/E'_{298} (i.e., the ratio of the storage modulus at temperature T to that at 298 K), normalized loss modulus E''_T/E''_{298} (i.e., the ratio of the loss modulus at temperature T to that at 298 K) and loss factor $\tan\delta$ of the $[(\text{CH}_3)_2\text{NH}_2][\text{Mg}(\text{HCOO})_3]$ pellet. Near the ferroelectric transition temperature of 264 K, the storage modulus of the single crystals and the normalized loss modulus of the pellet reached the minimum, and the loss modulus and loss factor of the $[(\text{CH}_3)_2\text{NH}_2][\text{Mg}(\text{HCOO})_3]$ single crystals and the normalized loss modulus and loss factor of the $[(\text{CH}_3)_2\text{NH}_2][\text{Mg}(\text{HCOO})_3]$ pellet reached the maximum. $[(\text{CH}_3)_2\text{NH}_2][\text{Mg}(\text{HCOO})_3]$ displays much narrower peaks of loss modulus, normalized loss modulus and loss factor near the ferroelectric transition temperature compared with $[\text{NH}_4][\text{Mg}(\text{HCOO})_3]$. The peak temperature tends to be independent of frequency, and the peak height tends to decrease with the increase in frequency, indicating the features of the first-order phase transition. The elastic anomalies and energy loss related to the ferroelectric transition in $[(\text{CH}_3)_2\text{NH}_2][\text{Mg}(\text{HCOO})_3]$ were similar to those reported for $[(\text{CH}_3)_2\text{NH}_2][\text{Mn}(\text{HCOO})_3]$ and $[(\text{CH}_3)_2\text{NH}_2][\text{Fe}(\text{HCOO})_3]$ investigated by DMA [39,53].

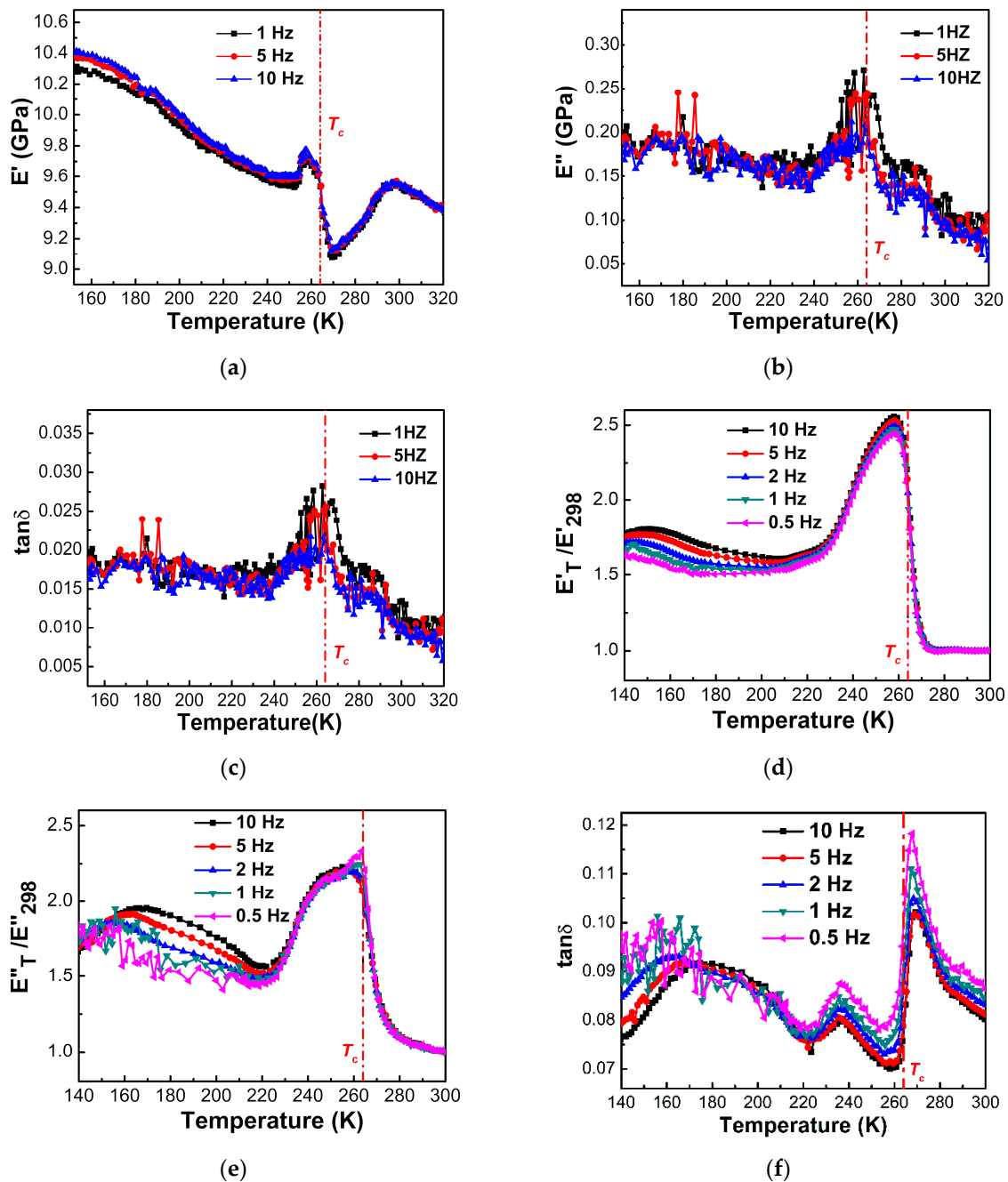


Figure 7. Temperature dependences of (a) storage modulus E' , (b) loss modulus E'' , (c) loss factor $\tan\delta$ of $[(\text{CH}_3)_2\text{NH}_2][\text{Mg}(\text{HCOO})_3]$ single crystals, (d) normalized storage modulus E'_T/E'_{298} , (e) normalized loss modulus E''_T/E''_{298} and (f) loss factor $\tan\delta$ of $[(\text{CH}_3)_2\text{NH}_2][\text{Mg}(\text{HCOO})_3]$ pellet determined by DMA during heating at the rate of 2 K/min. The vertical dash-dotted line indicates the ferroelectric transition temperature of 264 K.

Asaji et al. reported that the ferroelectric transition in $[(\text{CH}_3)_2\text{NH}_2][\text{Mg}(\text{HCOO})_3]$ was first order, and it was associated with the freezing of the 120° reorientation of the dimethylammonium ion around the c - c axis through the two methyl groups of the cation, which were non-equivalent below the ferroelectric transition temperature of 267 K [36]. The strong frequency dependence of the dielectric constant and the dielectric loss of $[(\text{CH}_3)_2\text{NH}_2][\text{Mg}(\text{HCOO})_3]$ were reported, and the peak temperature increased at higher frequencies, indicating a dielectric relaxation mechanism [35]. The RUS study of the elastic properties and acoustic dissipation associated with the disorder–order ferroelectric transition in $[(\text{CH}_3)_2\text{NH}_2][\text{M}(\text{HCOO})_3]$ ($\text{M} = \text{Mn}, \text{Co}, \text{Ni}$) exhibited a broadening of the

resonant peaks above the ferroelectric transition temperature and kinks in the temperature dependence of the resonant frequencies, which are proportional to elastic moduli, near the ferroelectric transition temperature of 185 K ($M = \text{Mn}$), 165 K ($M = \text{Co}$) and 180 K ($M = \text{Ni}$), respectively [40,41].

Figure 8 demonstrates a double logarithmic plot of the frequency dependence of loss factor peak height, $\ln(\tan\delta)$ vs. $\ln(f)$, for the peak in the temperature dependence of $\tan\delta$ near 256 K for $[\text{NH}_4][\text{Mg}(\text{HCOO})_3]$, and near 264 K for $[(\text{CH}_3)_2\text{NH}_2][\text{Mg}(\text{HCOO})_3]$. Two fitting processes were used to determine the values of $\tan\delta$. In the first case, the values are relative to the zero base line. In the second case, the values are relative to the base line near 150 K for $[\text{NH}_4][\text{Mg}(\text{HCOO})_3]$ and near 260 K for $[(\text{CH}_3)_2\text{NH}_2][\text{Mg}(\text{HCOO})_3]$. The decay is consistent with the power law $\tan\delta = Af^n$, where n is between -0.029 and -0.023 for $[\text{NH}_4][\text{Mg}(\text{HCOO})_3]$ and between -0.077 and -0.049 for $[(\text{CH}_3)_2\text{NH}_2][\text{Mg}(\text{HCOO})_3]$. Similar features were reported for $[(\text{CH}_3)_2\text{NH}_2][\text{Mn}(\text{HCOO})_3]$ with n between -0.382 and -0.078 [39].

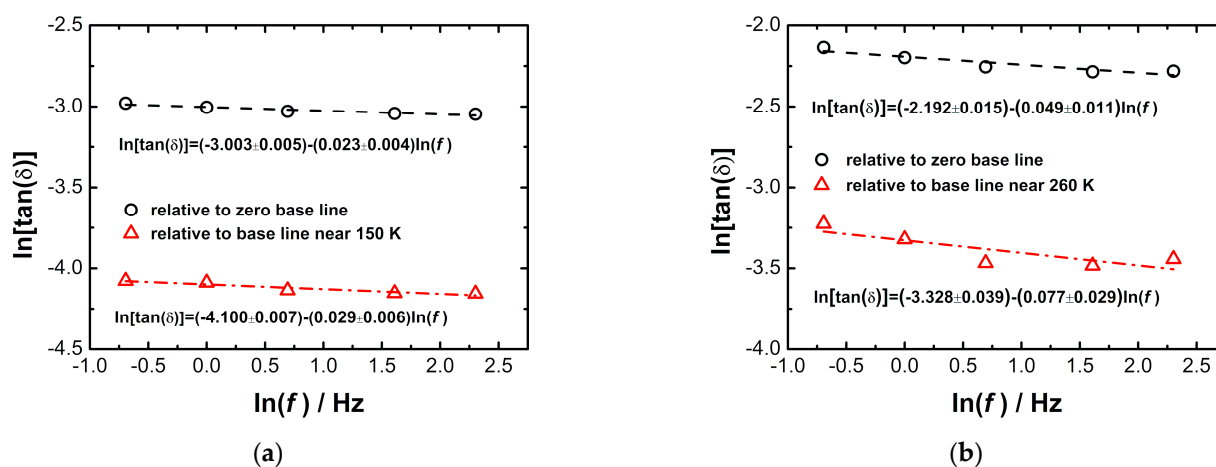


Figure 8. Double logarithmic plot $\ln(\tan\delta)$ vs. $\ln(f)$ for the peak in the temperature dependence of $\tan\delta$ near 260 K in $[\text{NH}_4][\text{Mg}(\text{HCOO})_3]$ (a) and near 270 K in $[(\text{CH}_3)_2\text{NH}_2][\text{Mg}(\text{HCOO})_3]$ (b).

The elastic anomalies and energy loss associated with the ferroelectric transitions were detected using BS at 0–30 GHz, RUS at 0.1–2.0 MHz and DMA at 0.1–10 Hz. This suggests that multiple relaxation processes may be involved with different relaxation times, e.g., around 10^{-12} s detected by BS, around 10^{-6} s detected by RUS and around 1 s detected by DMA.

4. Conclusions

DMA studies of the elastic properties and energy loss of multiferroic MOFs, $[\text{NH}_4][\text{Mg}(\text{HCOO})_3]$ and $[(\text{CH}_3)_2\text{NH}_2][\text{Mg}(\text{HCOO})_3]$, at low frequencies of 0.5 Hz to 10 Hz between 140 K and 320 K, illustrated the minimum in storage modulus and the maximum in loss modulus and loss factor near the ferroelectric transition temperatures of 256 K and 264 K, respectively. For $[\text{NH}_4][\text{Mg}(\text{HCOO})_3]$, the peaks of the loss modulus and loss factor were broad, and they displayed weak frequency dependence. $[(\text{CH}_3)_2\text{NH}_2][\text{Mg}(\text{HCOO})_3]$ showed much narrower peaks of loss modulus and loss factor. The peak temperature was independent of frequency, and the peak height decreased at higher frequencies, indicating the features of the first-order phase transition. The frequency dependence of the loss factor peak height was consistent with the power law $\tan\delta = Af^n$, where n was between -0.029 and -0.023 for $[\text{NH}_4][\text{Mg}(\text{HCOO})_3]$ and between -0.077 and -0.049 for $[(\text{CH}_3)_2\text{NH}_2][\text{Mg}(\text{HCOO})_3]$. The elastic anomalies and energy loss in $[\text{NH}_4][\text{Mg}(\text{HCOO})_3]$ near 256 K are due to the second-order paraelectric to ferroelectric phase transition triggered by the disorder–order transition of the ammonium cations and their displacement within the framework channels, accompanied by the structural phase transition from the non-polar hexagonal space group $P6_322$ to the polar hexagonal space group $P6_3$. The

elastic anomalies and energy loss in $[(\text{CH}_3)_2\text{NH}_2][\text{Mg}(\text{HCOO})_3]$ near 264 K are due to the first-order paraelectric to ferroelectric phase transitions triggered by the disorder–order transitions of alkylammonium cations located in the framework cavities, accompanied by the structural phase transition from rhombohedral space group $R\bar{3}c$ to monoclinic space group Cc . The elastic anomalies in $[\text{NH}_4][\text{Mg}(\text{HCOO})_3]$ and $[(\text{CH}_3)_2\text{NH}_2][\text{Mg}(\text{HCOO})_3]$ showed strong coupling of ferroelasticity with ferroelectricity. Multiple relaxation processes may be involved with different relaxation times, e.g., around 10^{-12} s detected by BS, around 10^{-6} s detected by RUS and around 1 s detected by DMA. Structure plays an important role in the elastic properties of MOFs. The study of the elastic anomalies and energy loss related to ferroelectric transitions is important for the development of multiferroic MOFs with high strength, ferroelectric transition temperature near room temperature, strong coupling of ferroelasticity, ferroelectricity and ferromagnetism for use in actuators, magnetic and electric devices.

Author Contributions: Conceptualization, Z.Z.; methodology, H.Y., X.S., L.S., S.Y. and H.T.; formal analysis, H.Y. and H.T.; investigation, Z.Z., H.Y. and H.T.; writing—original draft preparation, Z.Z., H.Y. and H.T.; writing—review and editing, Z.Z., H.Y., X.S., L.S., S.Y. and H.T.; supervision, Z.Z.; funding acquisition, Z.Z.; materials synthesis, H.Y., X.S., L.S., S.Y. and H.T.; XRD, H.Y., X.S. and H.T.; DSC, H.Y. and H.T.; DMA, H.Y., X.S., L.S., S.Y. and H.T. All authors have read and agreed to the published version of the manuscript.

Funding: This research was funded by the National Natural Science Foundation of China, grant number 51,502,229, and the Start-up Research Foundation of Wuhan University of Technology, grant number 101-40120189.

Institutional Review Board Statement: Not applicable.

Informed Consent Statement: Not applicable.

Data Availability Statement: The data presented in this study are available on request from the corresponding authors. The data are not publicly available due to privacy reasons.

Acknowledgments: The authors wish to thank Lipeng Xin, Xiaoming Wang and Dongpeng Cheng for their valuable discussions.

Conflicts of Interest: The authors declare no conflict of interest.

References

1. Cheetham, A.K.; Rao, C.N.R. There's room in the middle. *Science* **2007**, *318*, 58–59. [[CrossRef](#)] [[PubMed](#)]
2. Rao, C.N.R.; Cheetham, A.K.; Thirumurugan, A.J. Hybrid inorganic-organic materials, a new family in condensed matter physics. *Phys. Condens. Matter* **2008**, *20*, 083202. [[CrossRef](#)]
3. Spaldin, N.A.; Cheong, S.W.; Ramesh, R. Multiferroics, past, present and future. *Phys. Today* **2010**, *63*, 38–43. [[CrossRef](#)]
4. Reed, D.A.; Keitz, B.K.; Oktawiec, J.; Mason, J.A.; Runcevski, T.; Xiao, D.J.; Darago, L.E.; Crocella, V.; Bordiga, S.; Long, J.R. A spin transition mechanism for cooperative adsorption in metal-organic frameworks. *Nature* **2017**, *550*, 96–100. [[CrossRef](#)]
5. Han, X.; Godfrey, H.G.W.; Briggs, L.; Davies, A.J.; Cheng, Y.Q.; Daemen, L.L.; Sheveleva, A.M.; Tuna, F.; McInnes, E.J.L.; Sun, J.L.; et al. Reversible adsorption of nitrogen dioxide within a robust porous metal-organic framework. *Nat. Mater.* **2018**, *17*, 691–696. [[CrossRef](#)]
6. Shen, K.; Zhang, L.; Chen, X.D.; Liu, L.M.; Zhang, D.L.; Han, Y.; Chen, J.Y.; Long, J.L.; Luque, R.; Li, Y.W.; et al. Ordered macro-microporous metal-organic framework single crystals. *Science* **2018**, *359*, 206–210. [[CrossRef](#)]
7. Jiang, Z.; Xu, X.H.; Ma, Y.H.; Cho, H.S.; Ding, D.; Wang, C.; Wu, J.; Oleynikov, P.; Jia, M.; Cheng, J.; et al. Filling metal-organic framework mesopores with TiO_2 for CO_2 photoreduction. *Nature* **2020**, *586*, 549–554. [[CrossRef](#)]
8. Wang, Z.M.; Zhang, B.; Otsuka, T.; Inoue, K.; Kobayashi, H.; Kurmoo, M. Anionic NaCl -type frameworks of $[\text{Mn}^{\text{II}}(\text{HCOO})_3]^-$, templated by alkylammonium, exhibit weak ferromagnetism. *Dalton Trans.* **2004**, *15*, 2209–2216. [[CrossRef](#)]
9. Wang, Z.; Hu, K.; Gao, S.; Kobayashi, H. Formate-based magnetic metal-organic frameworks templated by protonated amines. *Adv. Mater.* **2010**, *22*, 1526–1533. [[CrossRef](#)]
10. Zhang, W.; Xiong, R. Ferroelectric metal-organic frameworks. *Chem. Rev.* **2012**, *112*, 1163–1195. [[CrossRef](#)]
11. Li, W.; Henke, S.; Cheetham, A.K. Research update, mechanical properties of metal-organic frameworks—influence of structure and chemical bonding. *APL Mater.* **2014**, *2*, 123902. [[CrossRef](#)]
12. Carpenter, M.A. Static and dynamic strain coupling behaviour of ferroic and multiferroic perovskites from resonant ultrasound spectroscopy. *J. Phys. Condens. Matter* **2015**, *27*, 263201–263223. [[CrossRef](#)]

13. Asadi, K.; Veen, M.A. Ferroelectricity in metal-organic frameworks, characterization and mechanisms. *Eur. J. Inorg. Chem.* **2016**, 4332–4344. [[CrossRef](#)]
14. Li, W.; Wang, Z.M.; Deschler, F.; Gao, S.; Friend, R.H.; Cheetham, A.K. Chemically diverse and multifunctional hybrid organic-inorganic perovskites. *Nat. Rev. Mater.* **2017**, *2*, 16099–16116. [[CrossRef](#)]
15. Maczka, M.; Pietraszko, A.; Macalik, B.; Kermanowicz, K. Structure, phonon properties, and order-disorder transition in the metal formate framework of $[\text{NH}_4][\text{Mg}(\text{HCOO})_3]$. *Inorg. Chem.* **2014**, *53*, 787–794. [[CrossRef](#)] [[PubMed](#)]
16. Zhang, Z.Y.; Li, W.; Carpenter, M.A.; Howard, C.J.; Cheetham, A.K. Elastic properties and acoustic dissipation associated with a disorder-order ferroelectric transition in a metal-organic framework. *CrystEngComm* **2015**, *17*, 370–374. [[CrossRef](#)]
17. Xu, G.C.; Ma, X.M.; Zhang, L.; Wang, Z.M.; Gao, S. Disorder-order ferroelectric transition in the metal formate framework of $[\text{NH}_4][\text{Zn}(\text{HCOO})_3]$. *J. Am. Chem. Soc.* **2010**, *132*, 9588–9590. [[CrossRef](#)]
18. Li, W.; Probert, M.R.; Kosa, M.; Bennett, T.D.; Thirumurugan, A.; Burwood, R.P.; Parinello, M.; Howard, J.A.K.; Cheetham, A.K. Negative linear compressibility of a metal-organic framework. *J. Am. Chem. Soc.* **2012**, *134*, 11940–11943. [[CrossRef](#)] [[PubMed](#)]
19. Maczka, M.; Kadlubanski, P.; Freire, P.T.C.; Macalik, B.; Paraguassu, W.; Hermanowicz, K.; Hanuza, J. Temperature- and pressure-induced phase transitions in the metal formate framework of $[\text{ND}_4][\text{Zn}(\text{DCOO})_3]$ and $[\text{NH}_4][\text{Zn}(\text{HCOO})_3]$. *Inorg. Chem.* **2014**, *53*, 9615–9624. [[CrossRef](#)] [[PubMed](#)]
20. Wang, Z.M.; Zhang, B.; Inoue, K.; Fujiwara, H.; Otsuka, T.; Kobayashi, H.; Kurmoo, M. Occurrence of a rare $4^9 \cdot 6^6$ structural topology, chirality, and weak ferromagnetism in the $[\text{NH}_4][\text{M}^{\text{II}}(\text{HCOO})_3]$ ($\text{M}=\text{Mn}, \text{Co}, \text{Ni}$) frameworks. *Inorg. Chem.* **2007**, *46*, 437–445. [[CrossRef](#)]
21. Xu, G.C.; Zhang, W.; Ma, X.M.; Chen, Y.H.; Zhang, L.; Cai, H.L.; Wang, Z.M.; Xiong, R.G.; Gao, S. Coexistence of magnetic and electric orderings in the metal-formate frameworks of $[\text{NH}_4][\text{M}(\text{HCOO})_3]$. *J. Am. Chem. Soc.* **2011**, *133*, 14948–14951. [[CrossRef](#)] [[PubMed](#)]
22. Maczka, M.; Ptak, M.; Kojima, S. Brillouin scattering study of ferroelectric transition mechanism in multiferroic metal-organic frameworks of $[\text{NH}_4][\text{Mn}(\text{HCOO})_3]$ and $[\text{NH}_4][\text{Zn}(\text{HCOO})_3]$. *Appl. Phys. Lett.* **2014**, *104*, 222903–222906. [[CrossRef](#)]
23. Lawler, J.M.M.; Manuel, P.; Thompson, A.L.; Saines, P.J. Probing ferroic transitions in a multiferroic framework family, a neutron diffraction study of the ammonium transition metal formates. *Dalton Trans.* **2015**, *44*, 11613–11620. [[CrossRef](#)]
24. Collings, I.E.; Bykov, M.; Bykova, E.; Tucker, M.G.; Petitgirard, S.; Hanfland, M.; Glazyrin, K.; Smaalen, S.V.; Goodwin, A.L.; Dubrovinsky, L.; et al. Structural distortions in the high-pressure polar phases of ammonium metal formates. *CrystEngComm* **2016**, *18*, 8849–8857. [[CrossRef](#)]
25. Volkova, L.M.; Marinin, D.V. Possibility of emergence of chiral magnetic soliton in hexagonal metal formate $[\text{NH}_4][\text{M}(\text{HCOO})_3]$ with $\text{M}^{2+} = \text{Mn}, \text{Fe}, \text{Co},$ and Ni and $\text{KCo}(\text{HCOO})_3$. *J. Supercond. Novel Magn.* **2016**, *29*, 2931–2945. [[CrossRef](#)]
26. Wang, X.J.; Gou, G.Y.; Wang, D.W.; Xiao, H.Y.; Liu, Y.; Zhang, M.; Dkhil, B.; Ren, X.B.; Lou, X.J. Structural, electronic and magnetic properties of metal-organic-framework perovskites $[\text{AmH}][\text{Mn}(\text{HCOO})_3]$, a first-principles study. *RSC Adv.* **2016**, *6*, 48779–48787. [[CrossRef](#)]
27. Peksa, P.; Zareba, J.K.; Ptak, M.; Maczk, M.; Gagor, A.; Pawlus, S.; Sieradzki, A. Revisiting a perovskite-like copper-formate framework $\text{NH}_4[\text{Cu}(\text{HCOO})_3]$: Order-disorder transition influenced by Jahn-Teller distortion and above room-temperature switching of the nonlinear optical response between two SHG-active states. *J. Phys. Chem. C* **2020**, *124*, 18714. [[CrossRef](#)]
28. Sun, Y.J.; Zhuo, Z.W.; Wu, X.J. Ferroelectricity and magnetism in metal-formate frameworks of $[\text{NH}_4][\text{M}(\text{HCOO})_3]$ ($\text{M} = \text{Sc}$ to Zn), a first-principles study. *RSC Adv.* **2016**, *6*, 113234–113239. [[CrossRef](#)]
29. Jain, P.; Dalal, N.S.; Toby, B.H.; Kroto, H.W.; Cheetham, A.K. Order-disorder antiferroelectric phase transition in a hybrid inorganic-organic framework with the perovskite architecture. *J. Am. Chem. Soc.* **2008**, *130*, 10450–10451. [[CrossRef](#)]
30. Besara, T.; Jain, P.; Dalal, N.S.; Kuhns, P.L.; Reyes, A.P.; Kroto, H.W.; Cheetham, A.K. Mechanism of the order-disorder phase transition, and glassy behavior in the metal-organic framework $[(\text{CH}_3)_2\text{NH}_2][\text{Zn}(\text{HCOO})_3]$. *Proc. Natl. Acad. Sci. USA* **2011**, *106*, 6828–6832. [[CrossRef](#)]
31. Asaji, T.; Ashitomi, K. Phase transition and cationic motion in a metal-organic perovskite, dimethylammonium zinc formate $[(\text{CH}_3)_2\text{NH}_2][\text{Zn}(\text{HCOO})_3]$. *J. Phys. Chem. C* **2013**, *117*, 10185–10190. [[CrossRef](#)]
32. Abhyankar, N.; Kweon, J.J.; Orio, M.; Bertaina, S.; Lee, M.; Choi, E.S.; Fu, R.; Dalal, N.S. Understanding ferroelectricity in the Pb-free perovskite-like metal organic framework $[(\text{CH}_3)_2\text{NH}_2]\text{Zn}(\text{HCOO})_3$, dielectric, 2D NMR, and theoretical studies. *J. Phys. Chem. C* **2017**, *121*, 6314–6322. [[CrossRef](#)]
33. Rossin, A.; Ienco, A.; Costantino, F.; Montini, T.; Credico, D.; Caparoli, M.; Gonsalvi, L.; Fornasiero, P.; Peruzzini, M. Phase transitions and CO_2 adsorption properties of polymeric magnesium formate. *Cryst. Growth Des.* **2008**, *8*, 3302–3308. [[CrossRef](#)]
34. Rossin, A.; Fairen-Jimenez, D.; Dulren, T.; Giambastiani, G.; Peruzzini, M.; Vitillo, J.G. Hydrogen uptake by $\{\text{H}[\text{Mg}(\text{HCOO})_3] \supset \cap [\text{NHMe}_2]_{\infty}\}$ and determination of its H_2 adsorption sites through Monte Carlo simulations. *Langmuir* **2011**, *27*, 10124–10131. [[CrossRef](#)] [[PubMed](#)]
35. Pato-Doldan, B.; Sanchez-Andujar, M.; Gomez-Aguirre, L.C.; Yanez-Vilar, S.; Lopez-Beceiro, J.; Gracia-Fernandez, C.; Haghighirad, A.A.; Ritter, F.; Castro-Garcia, S.; Senaris-Rodriguez, M.A. Near room temperature dielectric transition in the perovskite formate framework $[(\text{CH}_3)_2\text{NH}_2][\text{Mg}(\text{HCOO})_3]$. *Phys. Chem. Chem. Phys.* **2012**, *14*, 8498–8501. [[CrossRef](#)] [[PubMed](#)]
36. Asaji, T.; Yoshitake, S.; Ito, Y.; Fujimori, H. Phase transition and cationic motion in the perovskite formate framework $[(\text{CH}_3)_2\text{NH}_2][\text{Mg}(\text{HCOO})_3]$. *J. Mol. Struct.* **2014**, *1076*, 719–723. [[CrossRef](#)]

37. Maczka, M.; Da Silva, T.A.; Paraguassu, W.; Da Silva, K.P. Raman scattering studies of pressure-induced phase transitions in perovskite formates $[(\text{CH}_3)_2\text{NH}_2][\text{Mg}(\text{HCOO})_3]$ and $[(\text{CH}_3)_2\text{NH}_2][\text{Cd}(\text{HCOO})_3]$. *Spectrochim. Acta Part A* **2016**, *156*, 112–117. [[CrossRef](#)]
38. Szymborska-Malek, K.; Trzebiatowska-Gusowska, M.; Maczka, M.; Gagor, A. Temperature-dependent IR and Raman studies of metal-organic frameworks $[(\text{CH}_3)_2\text{NH}_2][\text{M}(\text{HCOO})_3]$ (M=Mg, Cd). *Spectrochim. Acta Part A* **2016**, *159*, 35–41. [[CrossRef](#)] [[PubMed](#)]
39. Zhang, Z.Y.; Tang, H.; Cheng, D.P.; Zhang, J.K.; Chen, Y.T.; Shen, X.; Yu, H.L. Strain coupling and dynamic relaxation in multiferroic metal-organic framework $[(\text{CH}_3)_2\text{NH}_2][\text{Mn}(\text{HCOO})_3]$ with perovskite structure. *Results Phys.* **2019**, *12*, 2183–2188. [[CrossRef](#)]
40. Thomson, R.I.; Jain, P.; Cheetham, A.K.; Carpenter, M.A. Elastic relaxation behavior, magnetoelastic coupling, and order-disorder processes in multiferroic metal-organic frameworks. *Phys. Rev. B* **2012**, *86*, 214304–214310. [[CrossRef](#)]
41. Xin, L.P.; Zhang, Z.Y.; Carpenter, M.A.; Zhang, M.; Jin, F.; Zhang, Q.M.; Wang, X.M.; Tang, W.H.; Lou, X.J. Strain coupling and dynamic relaxation in a molecular perovskite-like multiferroic metal-organic framework. *Adv. Funct. Mater.* **2018**, *28*, 1806013. [[CrossRef](#)]
42. Baker, P.J.; Lancaster, T.; Franke, I.; Hayes, W.; Blundell, S.J.; Pratt, F.L.; Jain, P.; Wang, Z.M.; Kurmoo, M. Muon spin relaxation investigation of magnetic ordering in the hybrid organic-inorganic perovskites $[(\text{CH}_3)_2\text{NH}_2]\text{M}(\text{HCOO})_3$, M=Ni, Co, Mn, Cu. *Phys. Rev. B* **2010**, *82*, 012407–012410. [[CrossRef](#)]
43. Nagabhushana, G.P.; Shivaramaiah, R.; Navrotsky, A. Thermochemistry of multiferroic organic-inorganic hybrid perovskites $[(\text{CH}_3)_2\text{NH}_2][\text{M}(\text{HCOO})_3]$ (M = Mn, Co, Ni, and Zn). *J. Am. Chem. Soc.* **2015**, *137*, 10351–10356. [[CrossRef](#)]
44. Jain, P.; Stroppa, A.; Nabok, D.; Marino, A.; Rubano, A.; Paparo, D.; Matsubara, M.; Nakotte, H.; Feibig, M.; Picozzi, S.; et al. Switchable electric polarization and ferroelectric domains in a metal-organic-framework. *NPJ Quantum Mater.* **2016**, *1*, 16012. [[CrossRef](#)]
45. Clune, A.J.; Hughey, K.D.; Lee, C.; Abhyankar, N.; Ding, X.; Dalal, N.S.; Whangbo, M.H.; Singleton, J.; Musfeldt, J.L. Magnetic field-temperature phase diagram of multiferroic $[(\text{CH}_3)_2\text{NH}_2]\text{Mn}(\text{HCOO})_3$. *Phys. Rev. B* **2017**, *96*, 104424. [[CrossRef](#)]
46. Ma, Y.; Cong, J.Z.; Chai, Y.S.; Yan, L.Q.; Shang, D.S.; Sun, Y. Large pyroelectric and thermal expansion coefficients in the $[(\text{CH}_3)_2\text{NH}_2]\text{Mn}(\text{HCOO})_3$ metal-organic framework. *Appl. Phys. Lett.* **2017**, *111*, 042901. [[CrossRef](#)]
47. Xin, L.P.; Fan, Z.; Li, G.H.; Zhang, M.; Han, Y.H.; Wang, J.; Ong, K.P.; Qin, L.; Zheng, Y.Z.; Lou, X.J. Growth of centimeter-sized $[(\text{CH}_3)_2\text{NH}_2][\text{Mn}(\text{HCOO})_3]$ hybrid formate perovskite single crystals and Raman evidence of pressure-induced phase transitions. *New J. Chem.* **2017**, *41*, 151–159. [[CrossRef](#)]
48. Malik, V.; Maity, S.; Chatterjee, R. Temperature dependent negative differential resistance behavior in multiferroic metal organic framework $[(\text{CH}_3)_2\text{NH}_2][\text{Mn}(\text{HCOO})_3]$ crystals. *Org. Electron* **2018**, *56*, 5–10. [[CrossRef](#)]
49. Collings, I.E.; Bykov, M.; Bykova, E.; Hanfland, M.; Smaalen, S.; Dubrovinsky, L.; Bykova, E. Disorder-order transitions in the perovskite metal-organic frameworks $[(\text{CH}_3)_2\text{NH}_2][\text{Mn}(\text{HCOO})_3]$ at high pressure. *CrystEngComm* **2018**, *20*, 3512–3521. [[CrossRef](#)]
50. Hu, L.; Wang, Z.; Wang, H.; Qu, Z.; Chen, Q.W. Tuning the structure and properties of a multiferroic metal-organic-framework via growing under high magnetic fields. *RSC Adv.* **2018**, *8*, 13675–13678. [[CrossRef](#)]
51. Zhou, H.T.; Pan, D.S.; Li, Y.; Li, D.; Choi, C.J.; Zhang, Z.D. Magnetic transitions in metal-organic frameworks of $[(\text{CH}_3)_2\text{NH}_2][\text{Fe}^{\text{II}}(\text{HCOO})_3]$, $[(\text{CH}_3)_2\text{NH}_2][\text{Co}^{\text{II}}(\text{HCOO})_3]$ and $[(\text{CH}_3)_2\text{NH}_2][\text{Fe}^{\text{III}}\text{Fe}^{\text{II}}(\text{HCOO})_6]$. *J. Magn. Magn. Mater.* **2020**, *493*, 165715. [[CrossRef](#)]
52. Ma, Y.; Wang, Y.X.; Cong, J.Z.; Sun, Y. Magnetic-field tuning of hydrogen bond order-disorder transition in metal-organic frameworks. *Phys. Rev. Lett.* **2019**, *122*, 255701. [[CrossRef](#)]
53. Zhang, Z.Y.; Shen, X.; Yu, H.L.; Wang, X.M.; Sun, L.; Yue, S.M.; Cheng, D.P.; Tang, H. Elastic properties and energy dissipation related to the disorder-order ferroelectric transition in a multiferroic metal-organic framework $[(\text{CH}_3)_2\text{NH}_2][\text{Fe}(\text{HCOO})_3]$ with a perovskite-like structure. *Materials* **2021**, *14*, 2403. [[CrossRef](#)]
54. Ma, Y.; Sun, Y. Multiferroic and thermal expansion properties of metal-organic frameworks. *J. Appl. Phys.* **2020**, *127*, 080901–080910. [[CrossRef](#)]
55. Yu, Z.P.; Liu, C.; Shen, Z.W.; Zhai, K. Pressure effect on order-disorder ferroelectric transition in a hydrogen-bonded metal-organic framework. *J. Phys. Chem. Lett.* **2020**, *11*, 9566–9571. [[CrossRef](#)]
56. Collings, I.E.; Vasiukov, D.M.; McCammon, C.A.; Dubrovinsky, L.; Cerantola, V.; Petitgirard, S.; Hubschle, C.B.; Schonleber, A.; Chernyshov, D.; Smaalen, S.; et al. Local structure of ferroic iron formates at low temperature and high pressure studies by Mossbauer spectroscopy. *J. Phys. Chem. C* **2019**, *123*, 21676. [[CrossRef](#)]
57. Simenas, M.; Balciunas, S.; Gonzalez-Nelson, A.; Kinka, M.; Ptak, M.; Van der Veen, M.A.; Maczka, M.; Banys, J. Preparation and Dielectric Characterization of P(VDF-TrFE) Copolymer Based Composites Containing Metal-Formate Frameworks. *J. Phys. Chem. C* **2019**, *123*, 16380. [[CrossRef](#)]
58. Ramakrishna, S.K.; Kundu, K.; Bindra, J.K.; Locicero, S.A.; Talham, D.R.; Reyes, A.P.; Fu, R.Q.; Dalal, N.S. Probing the dielectric transition and molecular dynamics in the metal-organic framework $[(\text{CH}_3)_2\text{NH}_2][\text{Mg}(\text{HCOO})_3]$ using high resolution NMR. *J. Phys. Chem. C* **2021**, *125*, 3441. [[CrossRef](#)]